ADVANCED OPTICAL MATERIALS
www.advopticalmat.de

A Surface Plasmon Enhanced Near-Infrared Nanophotodetector

Lin-Bao Luo, Yi-Feng Zou, Cai-Wang Ge, Kun Zheng, Dan- Dan Wang, Rui Lu, Teng-Fei Zhang, Yong-Qiang Yu, and Zhong-Yi Guo**

In this work, we present a plasmonic near infrared light photodetector for the detection of 980 nm illumination. The plasmonic photodetector is fabricated by modifying single layer graphene (SLG)/InP Schottky junction diode with SiO_2 encapsulated gold nanorods (SiO_2@AuNR), which can confine the incident NIR light by inducing obvious localized surface plasmon resonance, according to theoretical simulation based on finite element method. This study shows that after decoration with plasmonic SiO_2@AuNR, the device performance in terms of photocurrent and responsivity is considerably enhanced. In addition, the device exhibited a very fast respose rate which is able to monitor switching optical signals with a frequency as high as 1 MHz, suggesting a potential application for sensing high-frequency optical signals. This study manifests that the present plasmonic NIR photodetector will have great potential in future optoelectronic devices application.

1. Introduction

As an important range in electromagnetic wave, infrared light (IR) has been widely used for both military (e.g., navigation, night vision, aerospace, and weapons detection)[1] and civil purposes (e.g., communications, medical imaging, atmospheric sounding, pollution control, meteorology, and environmental monitoring).[2] To date, a number of narrow band-gap semiconductor materials including group III–V semiconductors (e.g., InP, InSb, and GaAs),[3–5] group II–VI semiconductors (CdTe),[6–8] group IV semiconductors (carbon nanotubes, Ge, and Si),[9–11] and ternary semiconductors (e.g., CdSeTe[12] and HgCdTe[13]) have been employed to fabricate numerous highly sensitive IR photodetectors (IRPDs) with different kinds of device geometries (quantum well IRPDs, quantum dots IRPD, and Schottky-barrier IRPD).[14] Among the various photosensitive semiconductor materials, indium phosphide (InP) with a direct band gap of 1.35 eV which corresponds to the near-infrared (NIR) light has received special research interest lately. Due to the unique property of InP nanostructures, including high thermal conductivity, high carrier mobility, large absorption coefficient in the near IR (NIR) range, easy synthesis, and excellent compatibility with modern Si technology, great efforts in the past decade have been devoted to the development of various highly sensitive NIRPDs with device configuration of p^+–i–n^+,[15] p–n,[16] InP/InAs quantum dot (QD), and so on.[17] These devices either exhibited large on/off ratio, high conductive gain, or fast response rate. Despite these progresses, it is undeniable that most of the InP nanostructure-based devices mentioned above normally suffered from low responsivity and detectivity, which is mainly owing to the relatively small photon absorption cross-section.

A possible solution to this dilemma is to introduce noble metal nanostructures (Au or Ag nanoparticles) within the devices. It has been widely reported that plasmonic metal nanoparticles can induce strong localized surface plasmon resonance (LSPR), which will lead to very strong electromagnetic field around their surfaces. By this token, noble metal nanoparticles such as AuNPs and AgNPs have been widely regarded as one of the most efficient light confining elements to boost the some light-harvesting related optoelectronic devices including light emitting diodes (LEDs),[18,19] nanoantennas,[20] solar cell,[21–23] photodetectors,[24,25] and photocatalysts.[26] Enlighted by these works, we herein report a highly sensitive NIR photodetector which was fabricated by decorating plasmonic nanostructures on the surface of a graphene/semiconductor hybrid heterojunction, which represents a new class of material system, and has lately enormously emerged as a highly promising building blocks for fabricating high performance optoelectronic devices including solar cell,[27–29] photodetectors,[30–32] lasers,[33,34] LEDs, and so on.[35,36] Both experimental analysis and theoretical simulation based on finite element method (FEM) reveal that the plasmonic SiO_2@AuNRs can induce obvious LSPR band at ≈980 nm. Further device analysis reveals that the as-assembled

Prof. L.-B. Luo, Y.-F. Zou, C.-W. Ge, K. Zheng, D.-D. Wang, R. Lu, T.-F. Zhang, Dr. Y.-Q. Yu
School of Electronic Science and Applied Physics and Anhui Provincial Key Laboratory of Advanced Functional Materials and Devices
Hefei University of Technology
Hefei, Anhui 230009, P. R. China
E-mail: luolb@hfut.edu.cn
Prof. Z.-Y. Guo
School of Computer and Information
Hefei University of Technology
Hefei, Anhui 230009, P. R. China
E-mail: guozhongyi@hfut.edu.cn

DOI: 10.1002/adom.201500701

© 2016 WILEY-VCH Verlag GmbH & Co. KGaA, Weinheim

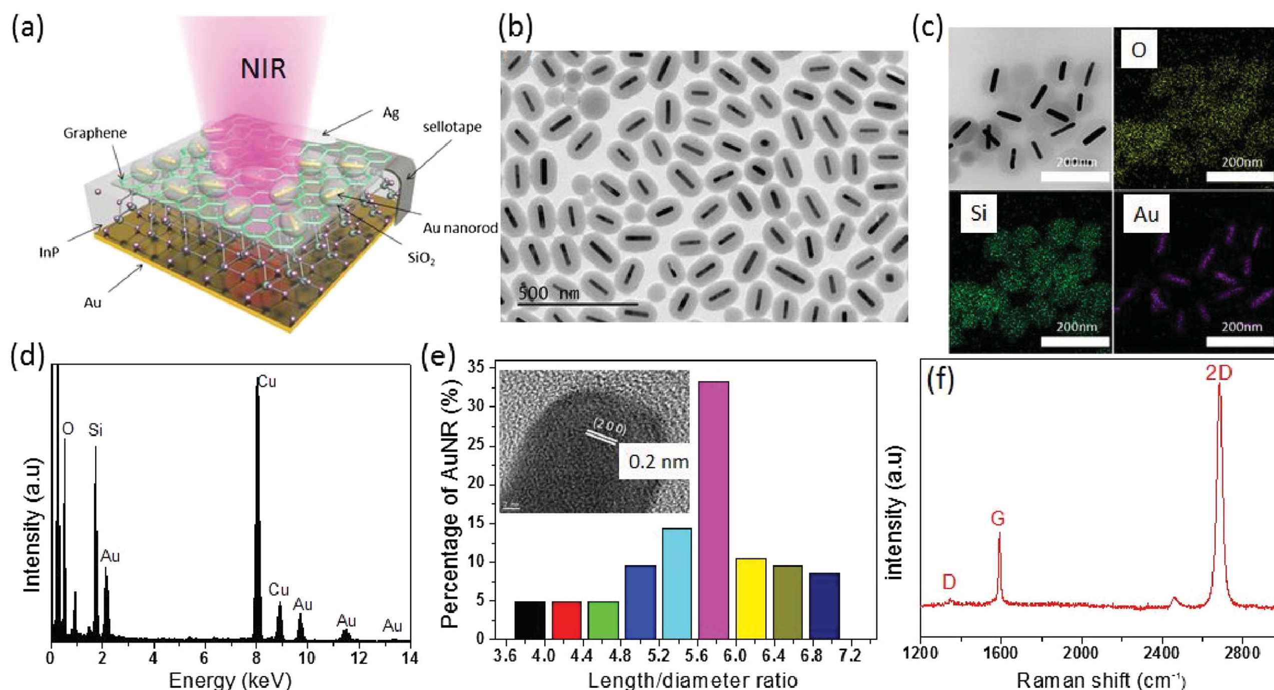

Figure 1. a) The schematic illustration of the SiO_2@AuNRs decorated SLG/InP NIRPD. b) TEM image of the SiO_2@AuNRs on SLG film. c) Elemental mapping profile of the SiO_2@AuNRs. d) EDS analysis of the SiO_2@AuNRs nanostructure. e) Statistical distribution of the length/diameter ratios of the SiO_2@AuNR, the inset shows a HRTEM image of a typical AuNR. f) Raman spectrum of the single-layer graphene film.

SiO_2 @AuNRs-single layer graphene (SLG)/InP diode exhibits typical photovoltaic behavior which makes it possible to detect 980 nm light at zero bias voltage with good reproducibility. It is also found that after modification with plasmonic SiO_2@AuNRs, some of the key parameters, including photocurrent, responsivity, and response rate, were considerably enhanced. We believed this study will offer new solutions to the development of high-performance optoelectronic devices in the future.

2. Results and Discussion

Figure 1a schematically shows the device geometry of the concept-of-proof NIRPD which is composed of n-type single crystalline InP wafer and SLG film decorated with SiO_2-coated AuNRs (SiO_2@AuNRs). From the transmission electron microscope (TEM) image shown in Figure 1b, it is seen that SLG layer has been covered a number of SiO_2@AuNRs, with a coverage ratio of 60%–70%. The shell/core SiO_2@AuNRs can be easily distinguished in the TEM image due to their distinctive difference in contrast (Figure 1c). The average length and diameter of the AuNRs are ≈89 and 16 nm, respectively, yielding an average aspect ratio (length/diameter) of 5.6 (Figure 1d). What is more, the length and diameter of the SiO_2 shell are ≈110 and 68 nm, respectively. Further elementary mapping profile of the Si, O, and Au atoms shows that the AuNRs are uniformly coated with SiO_2 layer (The strong Cu signal comes from the Cu grid during energy-dispersive X-ray spectroscopy study, EDS study). According to the high resolution TEM (HRTEM) shown in the inset of Figure 1e, the *d*-spacing of adjacent interplane perpendicular to the preferential growth orientation is calculated to be ≈0.20 nm, which corresponds to the (200) plane of Au (JCPDF No. 04-0784). Raman spectrum of the graphene layer in Figure 1f shows a 2D peak (≈2680 cm^{-1}) and a G peak (≈1590 cm^{-1}) with an intensity ratio of 2.42, indicative of the high quality of the SLG film. The weak D peak at ≈1340 cm^{-1} signifies a very low amount of defects.[37,38]

Theoretical simulation based on FEM was carried out to study the optical property of SiO_2@AuNR. **Figure 2**b shows the simulated absorption of the SiO_2@AuNR with different aspect ratios (the aspect ratio, namely L/W is defined as the length/width of the AuNRs; see Figure 2a). It is visible that all the SiO_2@AuNR structures exhibit strong absorption due to LSPR. Notably, when the L/W increases from 3 to 7.5, the absorption was observed to from visible light (700 nm) to near-infrared light (1150 nm). The observed LSPR bands are completely different from both Au nanospheres and Au nanoparticles, whose LSPR are usually located at ≈520 nm.[39] Such a shift can be ascribed to the high sensitivity of LSPR band to the surrounding dielectrics, as well the morphology of the nanostructures.[40] Figure 2d–f shows the electric field distribution of SiO_2@AuNR with L/W of 7.5, 5.6, and 3, respectively. One can see clearly that when shined by light illumination, all the SiO_2@AuNRs will act as an "optical antenna" that can trap the incident light as a result of plasmonic near-field coupling. Among the three kinds of core–shell nanostructures, the SiO_2@AuNRs with a L/W of 3 exhibits a relatively weak LSPR. In addition to the aspect ratio of AuNRs, the thickness of the SiO_2 sheath can tune the location of LSPR band as well. Figure 2c exhibits the theoretical absorption of the AuNRs coated by SiO_2 layer with thickness of 0, 40, 60, and 90 nm. Obviously, with the increase of SiO_2 thickness, the LSPR band will gradually redshift from

© 2016 WILEY-VCH Verlag GmbH & Co. KGaA, Weinheim

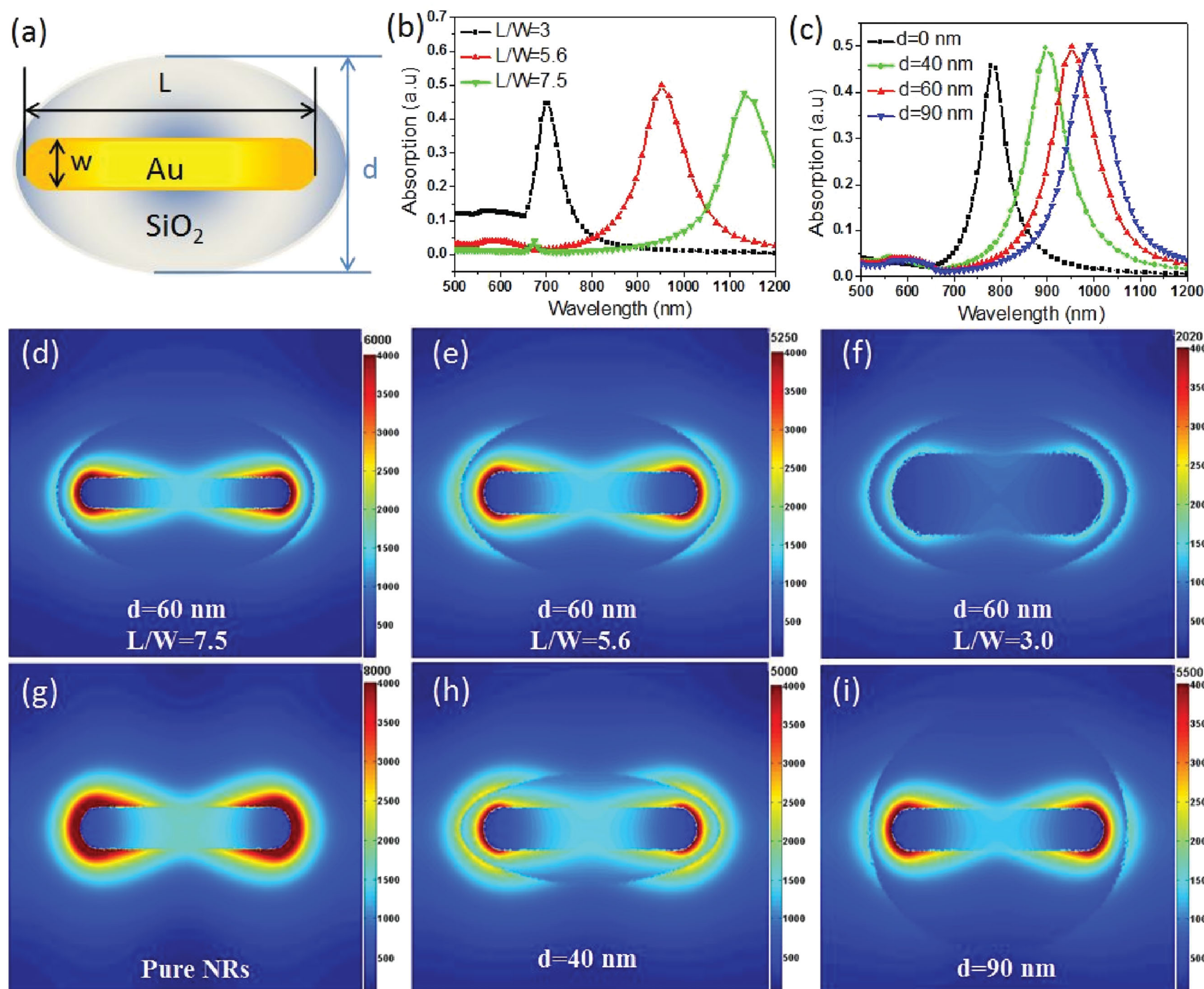

Figure 2. a) Schematic diagram of SiO_2@AuNRs model used in our simulation. b) Theoretical absorption curves of an individual SiO_2@AuNR with a constant SiO_2 thickness and aspect ratio of 7.5, 5.6, and 3.0, the corresponding electric field distribution (unit: W m^{-1}) is shown in (d)–(f), respectively. c) Theoretical absorption curves of individual SiO_2@AuNR with different SiO_2 thickness, the length/diameter ratio is set to be 5.6. The corresponding electric field distribution (unit: W m^{-1}) is shown in (g)–(i). The *E* field intensity of the light source in the simulation is 188.37 V m^{-1}.

900 to 1050 nm. Although these plasmonic nanostructures will slightly reduce the absorption of the SLG/InP heterojunction due to shading effect, the overall absorption of the SiO_2@AuNR-SLG/InP was obviously increased in comparison with that of the pure SLG/InP without any functional modification. More importantly, owing to the strong LSPR of the SiO_2@AuNR, the resulting near-field enhancement will be beneficial for the light detection.

Figure 3a plots the experimental absorption curves of SiO_2@AuNRs, and SLG/InP Schottky junction devices with and without surface decoration. It can be seen that the SLG/InP exhibits obvious enhancement of light absorption in the range from 600 to 1100 nm (the peak absorption is at ≈950 nm) after the decoration of SiO_2/AuNRs, which displays obvious absorption in that range. This result is in consistence with the theoretical simulation shown in Figure 3b. As a matter of fact, such an enhanced absorption due to surface modification is also verified by theoretical simulation of both devices based on FEM as shown in Figure 3c, from which one can see that the SiO_2@AuNRs with an aspect ratio of 5.6 can induce large-area and strong hot spots (area with high electric energy) when excited by light with a wavelength of 980 nm (Note that the *E* field intensity is dependent on the distance between SiO_2@AuNRs; see Figure S1 in the Supporting Information). Nonetheless, increasing or decreasing the irradiation wavelength will cause weak enhancement in electric field. In light of this, the present plasmonic device will be employed to detect illumination with wavelength of ≈980 nm.

To evaluate the effect of the plasmonic SiO_2@AuNRs on the optoelectronic property of InP Schottky junction, the current density–voltage (*J*–*V*) curve of the NIRPD with and without SiO_2@AuNRs in dark and under NIR light (λ = 980 nm, 6.7 mW cm^{-2}) was studied. As shown in **Figure 4**a, both devices show clear rectifying behavior. The corresponding rectification ratios are calculated to be 84.1 for the SLG/InP device and 69.7

© 2016 WILEY-VCH Verlag GmbH & Co. KGaA, Weinheim

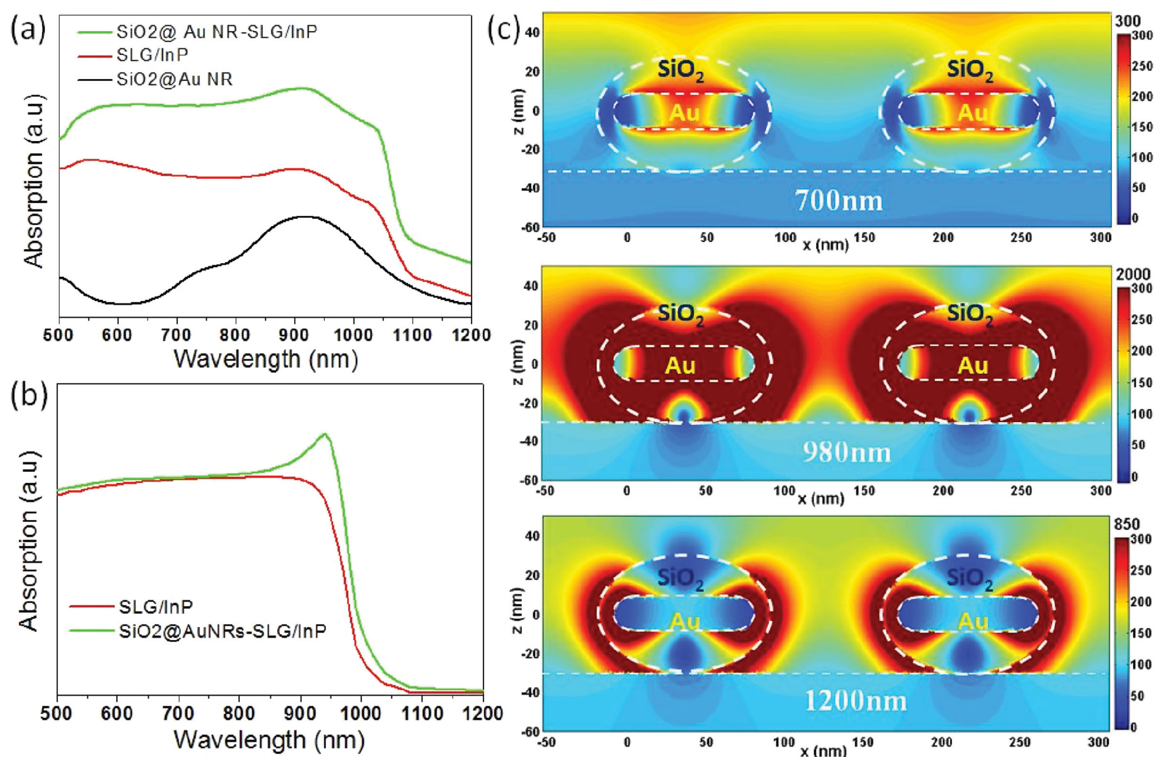

Figure 3. a) Experimental absorption curves of SiO_2@AuNRs, SLG/InP, and SiO_2@AuNRs decorated SLG/InP. b)Theoretical simulation of absorption of SLG/InP and SiO_2@AuNRs decorated SLG/InP. c) Electric field (unit: W m^{-1}) distribution of SLG/InP decorated with SiO_2@AuNRs under light illumination with wavelength of 700, 980, and 1200 nm, the aspect ratio of the simulated SiO_2@AuNRs is set to be 5.6.

for the SiO_2@AuNRs-SLG/InP, respectively. By fitting the *I–V* curves using thermionic emission base on diode equation (see the Supporting Information),[41] the Schottky barrier heights of SLG/InP and SiO_2@AuNRs-SLG/InP were estimated to be 0.75 and 0.70 eV, respectively. Such a slight increase in barrier height may be associated with increase of work function, which is obviously due to the surface decoration of SiO_2/AuNRs. Further careful examination of the *J–V* curves find that both devices exhibits apparent photovoltaic characteristic (inset of Figure 4a), the open-circuit voltage (V_{OC}) and the short-circuit current density (J_{SC}) are estimated to be 0.17/0.11 V and 207/65 µA cm^{-2} for SiO_2@AuNRs-SLG/InP and SLG/InP devices, respectively. As discussed later, the enhancement in both V_{OC} and J_{SC} is associated with the LSPR effect of SiO_2@AuNRs under 980 nm illumination. It should be pointed out that although the power conversion efficiency is very low (only ≈0.52%), the present plasmonic device can act as a low-consumption device that is capable of detecting NIR illumination without external power supply. Figure 4b shows the photoresponse of the two devices at zero bias voltage when illuminated by 980 nm illumination which were switched on and off alternatively. We can see that both devices can be readily switched between low and high resistance states with very good reproducibility. Specifically, the photocurrent for SiO_2@AuNRs decorated device is 101 µA which is much higher than that without decoration (29 µA), and the on/off ratios are estimated to be 776 and 230 for the decorated and undecorated devices, respectively. Further photocurrent study at different light intensity reveals that the photocurrent (I_p) of SiO_2@AuNRs-SLG/InP device exhibits high dependence on the intensity of excitation light. As exhibit in Figure 4c, the photocurrent of the plasmonic NIRPD increases gradually with the increasing illumination intensity. In fact, such a light intensity dependent photocurrent can be simply described by a simple power law: $I_p = AP^{\theta}$, where A is a constant for the incident light and the exponent θ ($0.5 < \theta < 1$) determines the response of photocurrent to light intensity. By fitting the equation to the experiment data, θ is estimated to be 0.95 (Figure 4d). This value close to 1 suggests the high quality of the device.[42,43]

The responsivity (*R*) and detectivity (*D*), two key device parameters for NIR photodetector, were calculated by the following equations

$$R(\mathrm{AW}^{-1}) = \frac{I_{\mathrm{photo}}}{P} = \eta\left(\frac{q\lambda}{hc}\right)G \quad (1)$$

$$D^{*} = R\sqrt{\frac{A_{\mathrm{opt}}}{2qI_{\mathrm{dark}}}} \quad (2)$$

where I_p is the photocurrent, I_d is the dark current, P_{opt} is the incident light power, η is the quantum efficiency (η = 3.96% for undecorated device and η = 14.70% for decorated device, respectively; see the Supporting Information),[40,44] h is the Planck constant (6.626×10^{-34} J s), c is the speed of light (2.997×10^{8} m s^{-1}), λ *is* the light wavelength (980 nm), A is the active area of the device, and q is the unit of elementary charge (1.6×10^{-19} C), respectively. In this study, the light intensity is 6.7 mW cm^{-2}, and the area of the SiO_2@AuNRs-SLG/InP

© 2016 WILEY-VCH Verlag GmbH & Co. KGaA, Weinheim

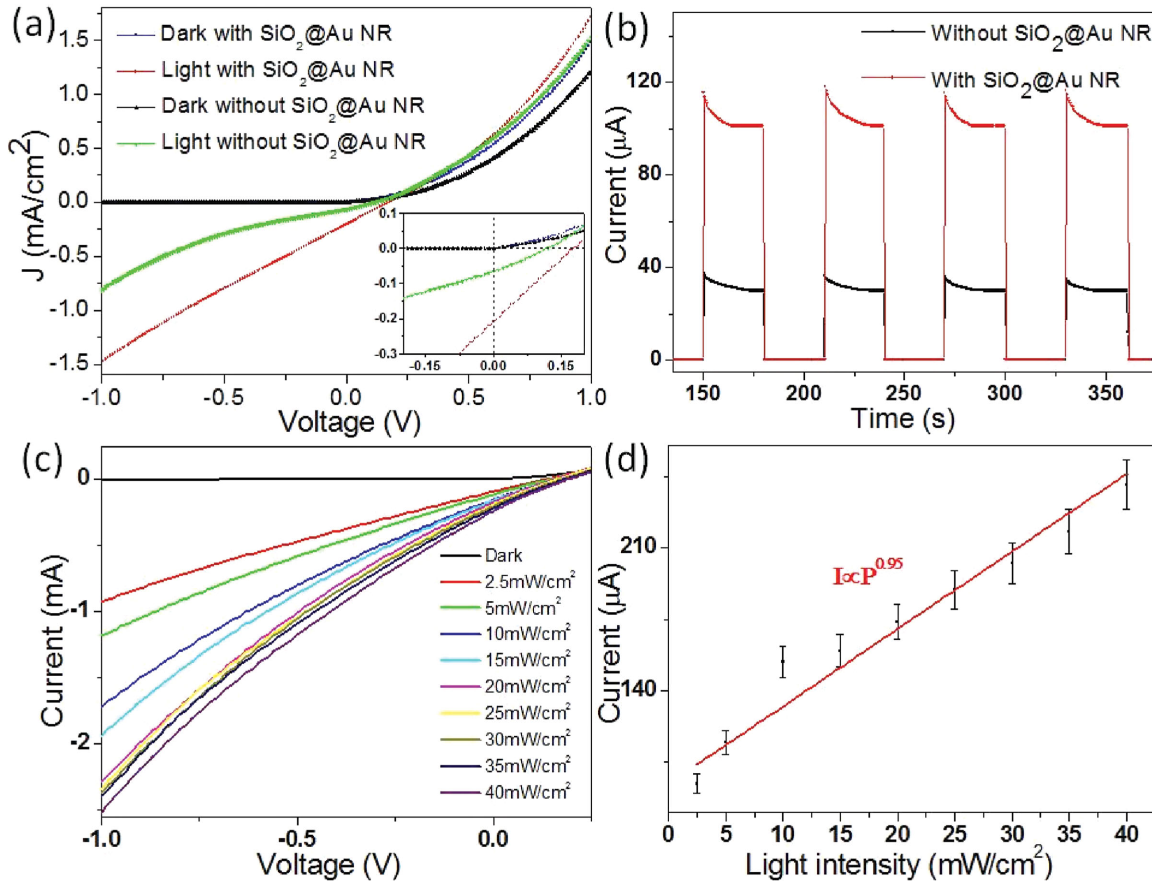

Figure 4. a) Typical *I–V* characteristics of the SLG/InP and the SLG/InP decorated with SiO_2@AuNRs, the inset shows the photovoltaic characteristics near the zero bias, the light intensity is 6.7 mw cm^{-2}. b) Photoresponse of two representative devices with and without SiO_2@AuNRs modification under 980 nm light illumination at $V_{bias} = 0$ V, the light intensity is 6.7 mW cm^{-2}. c) Photoresponse of the SiO_2@AuNRs decorated SLG/InP NIRPD under various light intensities. d) The fitting of the relationship between the photocurrent and light intensity.

NIRPD is ≈0.63 cm^2 (the device area is the the Schottky junction area where graphene is in contact with the InP wafer). Based on the above values, the R and D^* were estimated to be 139.8 mA W^{-1} and 10.5 × 10^{10} cm $Hz^{1/2}$ W^{-1}, respectively, which are much better than the device without SiO_2@AuNRs decoration (46.0 mA W^{-1} and 10.5 × 10^{10} cm $Hz^{1/2}$ W^{-1}). The two parameters are comparable to or relatively smaller than other InP material-based NIR photodetectors.

Another figure of merit for the NIRPD is the linear dynamic range (LDR, normally quoted in dB) which is given by

$$\mathrm{LDR} = 20\log\frac{I_{\mathrm{photo}}}{I_{\mathrm{dark}}} \quad (3)$$

where I_{photo} is the photocurrent measured at a light intensity of 1 mW cm^{-2}. By using the above equation, the LDR is estimated to be 51.7 dB which is comparable to other NIRPDs based on solution-processed PdS nanocrystals (60 dB),[45] copper phthalocyanine (CuPc) nanowires (35 dB),[46] and InGaAs film (66 dB), but lower than that of Si-based device (120 dB).[47] This modest value suggests great room for further device optimization. To gain a more accurate view of the actual *LDR* and precisely find out the minimum optical power which the present device can distinguish from the noise, we measured the noise current to calculate the noise equivalent power (NEP) by the following equation

$$\mathrm{NEP} = \frac{\sqrt{A_{\mathrm{opt}}\mathrm{BW}}}{D^*} = \frac{i_{\mathrm{n}}}{R} \quad (4)$$

where A_{opt} is the PD area, BW is the bandwidth of the PD, D^* is the detectivity, R is the responsivity, and i_n is the noise current, which is measured using a lock-in amplifier, respectively.[48] The noise current at different frequencies is plotted in **Figure 5**. Based on these values, the NEP is calculated to be 3.75 × 10^{-12} W $Hz^{-1/2}$. This value is much poorer than InAs/AlSb/GaSb millimeter-wave detector (0.24 pW $Hz^{-1/2}$),[49] but higher than the GaN/AlGaN/GaN p–i–n ultraviolet photodetector (8.3 pW $Hz^{-1/2}$).[50]

In addition to the modest LDR and low NEP, the present plasmonic device had a fast response rate. **Figure 6**a shows the photoresponse of the device under pulsed light illumination which is generated by a 980 nm laser diode driven by a high-frequency signal generator. It can be seen that the device can be repeatedly switched between high and low conductance states with excellent reproducibility even under a light pulse with frequency

© 2016 WILEY-VCH Verlag GmbH & Co. KGaA, Weinheim

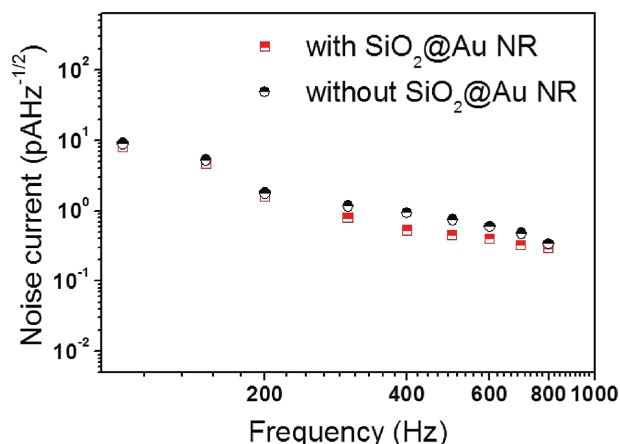

Figure 5. Noise current at different frequencies.

as high as 1 MHz. According to the normalized photocurrent at different frequencies shown in Figure 6c, the 3 dB bandwidth is estimated to be 104 kHz (corresponding to the frequency when the normalized photocurrent decreases from 1 to 0.707[51]). This value is comparable to organohalide perovskite photodetector (100 kHz)[46] but much higher than the devices without decoration (9200 Hz), and II–VI group semiconducting CdS nanoribbon device (369 Hz). [52] To further evaluate the response rate of the plasmonic NIRPD, one single cycle of photoresponse under 1 MHz light illumination was plotted in Figure 6b. By deducing the rise and fall edges, the rise time (τ_r, time interval for the photocurrent to rise from 10% to 90%) and the fall time (τ_f, time interval for the photocurrent to decrease from 90% to 10%) were estimated to be 442 and 433 ns, respectively. Such fast response rates are much faster than the SLG/InP without SiO_2@AuNRs (τ_r = 25.9 µs and τ_f = 43.3 µs, see Figure 6b). In fact, similar phenomena have been observed in other plasmonic metal–semiconductor nanostructures such as Ag–ZnO,[53] Au–CdTe,[7] and Au–ZnO as well.[54] According to these studies, such an increase in response rate is probably due to the suppressed exciton recombination after surface modification. Figure 6d compares the spectral response of the SLG/InP Schottky junction devices with and without surface modification. It is seen that both devices show apparent sensitivity to the illumination in the range from 350 to 1100 nm, with peak sensitivity at 950 nm. However, both of them are virtually blind

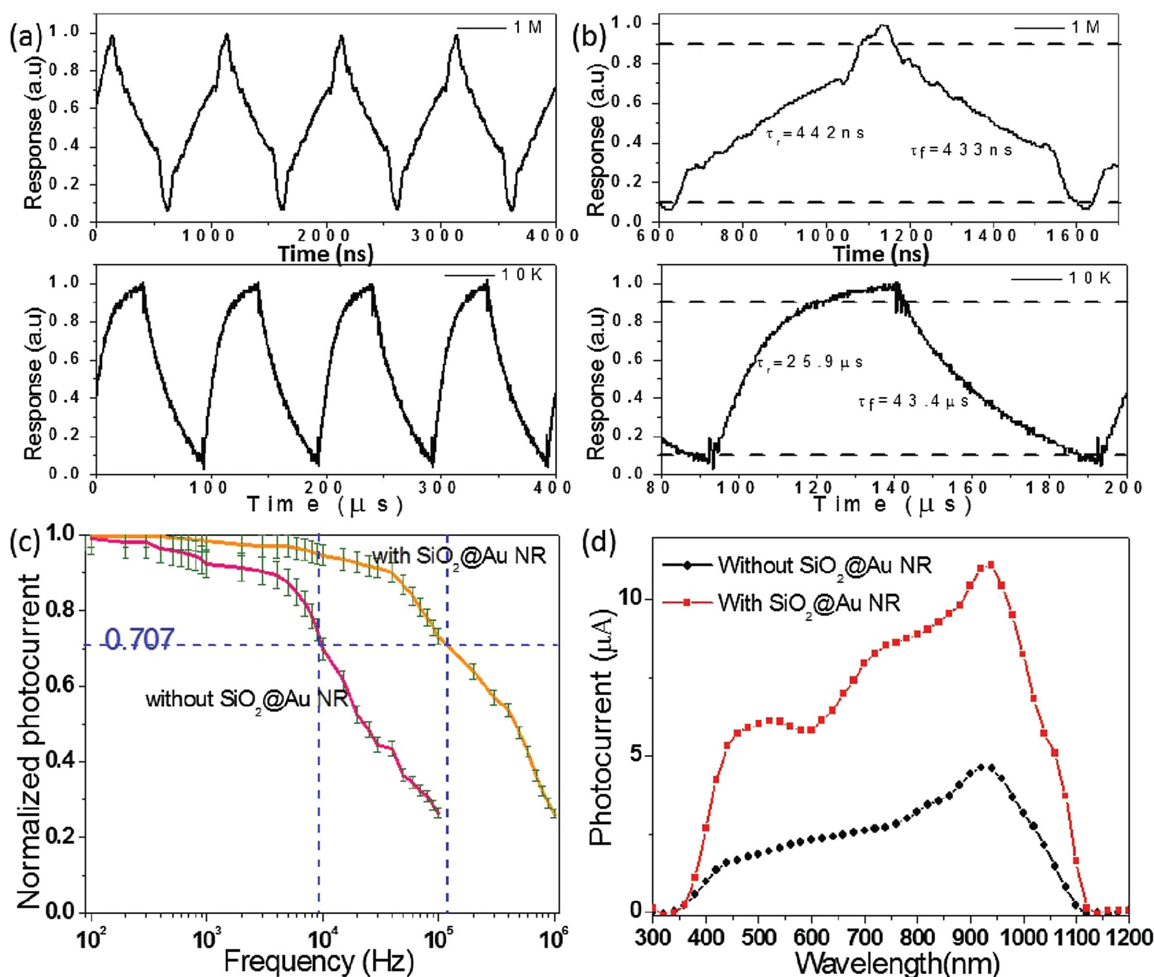

Figure 6. a) Photoresponse of a SiO_2@AuNR-SLGF/InP device to pulsed NIR irradiation at a frequency of 100 Hz and 1 MHz. b) The normalized photocurrent versus switching frequency. c) One normalized cycle measured at 1 MHz for estimating both rise time (τ_r) and fall time (τ_f). d) Spectral response of the NIRPD with and without decoration.

© 2016 WILEY-VCH Verlag GmbH & Co. KGaA, Weinheim

Table 1. Summary of the device performance of the present NIRPD and other InP nanostructure-based devices.

Materials	Responsivity	τ_r/τ_f	Detectivity Jones	Reference
SLG/InP	46.1 mA W^{-1}	25.9/43.3 µs	3.62×10^9	This work
SLG/InP with silica@AuNR	139.8 mA W^{-1}	441/433 ns	1.05×10^{10}	This work
InP/InAs QD	<100 mA W^{-1}	–	1.38×10^7	[55]
InP nanowire	19×10^4 A W^{-1}	0.04/1.13 s	–	[56]
InP/InGaAs quantum well	200 mA W^{-1}	–	$<1 \times 10^{10}$	[57]

to irradiation with wavelength larger than 1100 nm or less than 300 nm. Interestingly, in comparison with the device without decoration,SiO_2@AuNRs-SLG/InP shows an extra sensitivity at a peak of 500 nm, in consistence with the weak absorption peak shown in Figure 2a. **Table 1** summarizes some of the key metrics of the present NIRPD and other similar devices. One can see that, although the responsivity of the present plasmonic device did not show any obvious advantage, other parameters in terms of the response rate and detectivity are superior to other devices based on the InP nanowire (NW) and InP/InGaAs quantum wire (QW). These excellent device parameters and good spectral selectivity render our device a potential building block for future optoelectronic device applications.

Understandably, the enhanced photocurrent and responsivity are related to the following working mechanism. **Figure 7** shows the energy band diagram of SLG/InP which has a built-in potential formed near the interface, due to the different work functions between the SLG and InP. When irradiated by NIR illumination, the photogenerated holes–electron (h^+–e^-) pairs can be separated by the built-in electric field. The separated carriers were then transferred to the external circuit through the contact materials. This photoconductivity effect happens on condition that the energy of the incident photons is larger than the bandgap of InP (1.34 eV, 920 nm), which can explain well the poor sensitivity to irradiation with wavelength longer than ≈1000 nm. Notably, the decoration of SiO_2@AuNRs will influence the device performance of SLG/InP Schottky junction

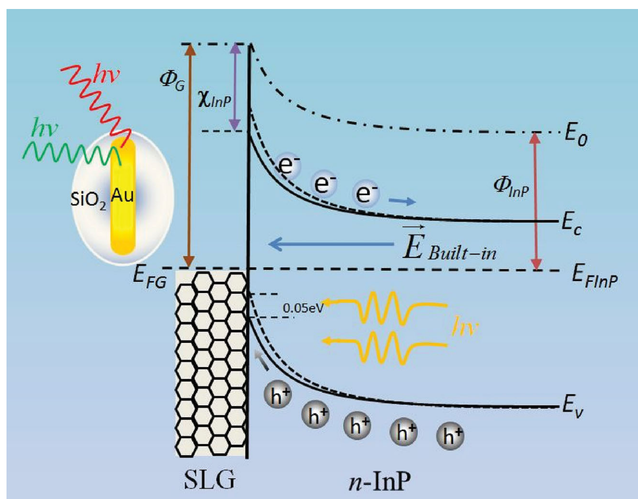

Figure 7. Energy band diagram of the NIR photodetector under light illumination.

NIRPD in the following two aspects. (1) The decoration will slightly increases the Schottky junction barrier from 0.7 to 0.75 eV. As a result, the built-in electric field is strengthened which is beneficial for the efficient separation of hole–electron pairs. (2) Under 980 nm light illumination, the incident light will be easily confined nearly SiO_2@AuNRs-SLG/InP device, such a light trapping effect will enhance the absorption of incident light, leading to the generation of more holes (h^+)–electrons (e^-) pairs and therefore larger photocurrent in comparison with that without SiO_2@AuNRs decoration. It should be noted that although a well-defined electron emission theory had been proposed to account for the enhanced photoelectric effect after modification with plasmonic nanoparticle,[55] unfortunately, this theory is not applicable to this study in that the AuNRs are not in direct contact with the SLG/InP Schottky junction diode. The presence of the insulating SiO_2 nanoshell will unfavorably prevent the transfer of electrons from plasmonic AuNR to SLG/InP.

3. Conclusion

In summary, we reported a high-performance NIRPD which was fabricated by coating SLG/InP Schottky junction diode with plasmonic SiO_2@AuNRs. Optoelectronic analysis reveals that after surface modification with SiO_2@AuNR, some of key metrics including responsivity, detectivity, and response time were considerably increased. Furthermore, the linear dynamic range and noise equivalent power were estimated to be 51.7 dB and 3.75×10^{-12}W Hz$^{-1/2}$, respectively, which are much better than other device with similar geometry. Theoretical simulation of the SiO_2@AuNR decorated SLG/InP based on FEM reveals that the optimized device performance is related to the light confinement effect and localized field enhancement of the SiO_2@AuNRs. This study suggests that the plamonic nanoparticle decorated NIRPD will have potential application in future optoelectronic devices.

4. Experimental Section

Preparation and Characterization of Silica-Coated AuNRs and SLG Film: The SiO_2-coated AuNRs were prepared by the following two steps: First, AuNRs were synthesized via a seed-mediated growth method in a binary surfactants mixture of hexadecyltrimethyl ammonium bromide (CTAB) and sodium oleate in aqueous solution. Second, the silica coating was realized via a base-catalyzed hydrolysis of tetraethyl orthosilicate (TEOS), in which the silica will deposit onto the surface of the AuNRs. Briefly, 0.25 mL of colloidal AuNRs in the first step was added into a

© 2016 WILEY-VCH Verlag GmbH & Co. KGaA, Weinheim

mixed solution composed of 15 mL H_2O, 8mL EtOH, and 2.4 mL stock CTAB solution under rigorously stirring for 30 min. The stock CTAB was prepared by adding 2 g CTAB in a solution of 16.6 mL EtOH and 135 mL H_2O, stirring at 50 °C for 30 min to be completely dissolved. Ammonium solution (3%) was then added to adjust the pH to ≈10 which is checked by using pH paper in order to avoid bubble. At last, 1.1 mL TEOS was added to the solution. The reaction was completed after 24 h under rigorously stirring at room temperature. The SLG films were grown upon 20 µm thick Cu foils through a chemical vapor deposition method by using a mixed gas of CH_4 (40 standard cubic centimeter per minute SCCM) and H_2 (20 SCCM) as reaction source at 1000 °C. After growth, the SLG films were spin coated with 5 wt% polymethylmethacrylate in chlorobenzene and then the underlying Cu foil was been removed by Marble's reagent solution ($CuSO_4$: HCl: H_2O = 10 g:50 mL:50 mL).

Device Construction and Characterization: To fabricate the SiO_2@AuNRs-SLG/InP Schottky junction photodetector, single crystalline n-type InP wafer (the carrier concentration is 3×10^{16} cm^{-3}) was first treated by 10% HCl solution for 30 s to remove the native oxide. Then, an Au film was deposited on the unpolished face of InP wafer as one electrode. A piece of sellotape was then placed at the edges of the as-treated InP wafer for the sake of insulation. After that, the above SLG was transferred onto the polished face of InP wafer and a drop of silver paste was wiped on the SLG. In order to modify the SLG/InP interface, 0.8 mg of dry SiO_2@AuNRs was first added into a 5 mL of absolute alcohol solution under vigorous stirring. After being stirred for more than 10 min, the resulting suspension (≈1 mL) was continuously dropped on the SLG/InP interface by a micropipette with a volume of 50 µL. The electrical characteristics of the NIRPD was carried out on a Keithley 4200-SCS semiconductor characterization system. During study, a 980 nm laser (Thorlabs-PPL1055T) was selected as the light source. To evaluate the response rate of the NIRPD, a home-built setup in which the fast-switching optical signal was achieved by a laser diode driven by a high-frequency signal generator and detected by an oscilloscope (Tektronix, TDS2012B).

Theoretical Simulation: The theoretical simulations of the optical responses of the selected simulating unit cell were carried out by the FEM. The refractive index of SiO_2 is 1.46, and the permittivity of Au and InP are obtained from luxpop. The size of the nanoparticles in the model is set to be identical to that obtained from scanning electron microscope (SEM) image. During calculation, we set the perfect magnetic conductor boundaries and perfect electrical conductor in the corresponding boundary of the model. The perfectly matching layers are utilized at the calculated region boundaries to reduce the influence of light reflection. A stationary solver is built to solve different frequency light coupling effect with plasmonic nanostructures.

Supporting Information

Supporting Information is available from the Wiley Online Library or from the author.

Acknowledgements

The authors appreciate Professor Qiao Zhang from Soochow University for providing the samples. This work was supported by the Natural Science Foundation of China (NSFC, Grant Nos. 61575059, 61575060, 21101051), the Natural Science Foundation of Anhui Province (Grant No. J2014AKZR0059), and the Fundamental Research Funds for the Central Universities (Grant Nos. 2012HGCX0003, 2013HGCH0012, 2014HGCH0005, and 2015HGCH0010).

Received: November 26, 2015
Revised: December 29, 2015
Published online: February 29, 2016

[1] C. Downs, T. E. Vandervelde. *Sensors* **2013**, *13*, 5054.
[2] S. Krishna, *Infrared Phys. Technol.* **2005**, *47*, 153.
[3] J. S. Miao, W. D. Hu, N. Guo, Z. Y. Lu, X. M. Zou, L. Liao, S. X. Shi, P. P. Chen, Z. Y. Fan, J. C. Ho, *ACS Nano* **2014**, *8*, 3628.
[4] M. A. Seyedi, M. J. Yao, J. O'brien, S. Y. Wang, P. D. Dapkus, *Appl. Phys. Lett.* **2014**, *105*, 041105.
[5] J. S. Miao, W. D. Hu, N. Guo, Z. Y. Lu, X. Q. Liu, L. Liao, P. P. Chen, T. Jiang, S. W. Wu, J. C. Ho, L. Wang, X. S. Chen, W. Lu, *Small* **2015**, *11*, 936.
[6] H. T. Wei, Y. J. Fang, Y. B. Yuan, L. Shen, J. S. Huang, *Adv. Mater.* **2015**, *27*, 4975.
[7] L. B. Luo, X. L. Huang, M. Z. Wang, C. Xie, C. Y. Wu, J. G. Hu, L. Wang, J. A. Huang, *Small* **2014**, *10*, 1645.
[8] Q. S. Wang, M. Safdar, Z. X. Wang, J. He, *Adv. Mater.* **2013**, *25*, 3915.
[9] M. S. Arnold, J. D. Zimmerman, C. K. Renshaw, X. Xu, R. R. Lunt, C. M. Austin, S. R. Forrest, *Nano Lett.* **2009**, *9*, 3365.
[10] L. H. Zeng, M. Z. Wang, H. Hu, B. Nie, Y. Q. Yu, C. Y. Wu, L. Wang, J. G. Hu, C. Xie, F. X. Liang, L. B. Luo, *ACS Appl. Mater. Interfaces* **2013**, *5*, 9362.
[11] L. B. Luo, L. H. Zeng, C. Xie, Y. Q. Yu, F. X. Liang, C. Y. Wu, L. Wang, J. G. Hu, *Sci. Rep.* **2014**, *4*, 3914.
[12] P. S. Wijewarnasuriya, Y. Chen, G. Brill, B. Zandi, N. K. Dhar. *IEEE Trans. Electron Devices* **2010**, *57*, 782.
[13] J. Wang, X. S. Chen, W. D. Hu, L. Wang, W. Lu, F. Q. Xu, J. Zhao, Y. L. Shi, R. B. Ji, *Appl. Phys. Lett.* **2011**, *99*, 113508.
[14] S. D. Gunapala, D. R. Rhiger, C. Jagadish, *Advances in Infrared Photodetectors*, Elsevier, Dublin, Ireland, **2011**.
[15] V. Jain, A. Nowzari, J. Wallentin, M. T. Borgstrom, M. E. Messing, D. Asoli, M. Graczyk, B. Witzigmann, F. Capasso, L. Samuelson, *Nano Res.* **2014**, *7*, 544.
[16] M. N. Amin, O. Alam, *J. Commun.* **2012**, *7*, 808.
[17] H. Lim, S. Tsao, W. Zhang, M. Razeghi, *Appl. Phys. Lett.* **2007**, *90*, 131112.
[18] A. Kock, E. Gornik, M. Hauser, W. Beinstingl, *Appl. Phys. Lett.* **1990**, *57*, 2327.
[19] K. Okamoto, I. Niki, A. Shvartser, Y. Narukawa, T. Mukai, A. Scherer, *Nat. Mater.* **2004**, *3*, 601.
[20] B. J. Roxworthy, K. D Ko, A. Kumar, K. H. Fung, E. K. C. Chow, G. L. Liu, N. X. Fang, K. C. Toussaint, *Nano Lett.* **2012**, *12*, 796.
[21] H. A. Atwater, A. Polman, *Nat. Mater.* **2010**, *9*, 205.
[22] H. R. Tan, R. Santbergen, A. H. M. Smets, M. Zeman, *Nano Lett.* **2012**, *12*, 4070.
[23] K. P. Catchpole, A. Polman, *Opt. Express* **2008**, *16*, 21793.
[24] M. W. Knight, H. Sobhani, P. Nordlander, N. J. Halas, *Science* **2011**, *332*, 702.
[25] J. S. Miao, W. D. Y. L. Jing, W. J. Luo, L. Liao, A. L. Pan, S. W. Wu, J. X. Cheng, X. S. Chen, W. Lu, *Small* **2015**, *11*, 2392.
[26] W. T. Kung, Y. H. Pai, Y. K. Hsu, C. H. Lin, C. M. Wang, *Opt. Exp.* **2013**, *21*, 221.
[27] Y. Song, X. M. Li, C. Mackin, X. Zhang, W. J. Fang, T. Palacios, H. W. Zhu, J. Kong, *Nano Lett.* **2015**, *15*, 2104.
[28] C. Xie, J. S. Jie, B. Nie, T. X. Yan, Q. Li, P. Lv, F. Z. Li, M. Z. Wang, C. Y. Wu, L. Wang, *Appl. Phys. Lett.* **2012**, *100*, 193103.
[29] L. H. Zhang, L. L. Fan, Z. Li, E. Z. Shi, X. M. Li, H. B. li, C. Y. Ji, Y. Jia, J. Q. Wei, K. L. Wang, H. W. Zhu, D. H. Wu, A. Y. Cao, *Nano Res.* **2011**, *4*, 891.
[30] M. Amirmazlaghani, F. Raissi, O. Habibpour, J. Vukusic, *IEEE J. Quantum Electron.* **2013**, *49*, 589.
[31] X. H. An, F. Z. Liu, Y. J. Jung, S. Kar, *Nano Lett.* **2013**, *13*, 909.
[32] J. W. Liu, R. T. Lu, G. W. Xu, J. Wu, P. Thapa, D. Moore, *Adv. Funct. Mater.* **2013**, *23*, 4941.
[33] J. T. Li, M. M. Jiang, C. X. Xu, Y. Y. Wang, Y. Lin, J. F. Lu, Z. L. Shi, *Sci. Rep.* **2015**, *5*, 9263.

© 2016 WILEY-VCH Verlag GmbH & Co. KGaA, Weinheim

[34] J. T. Li, Y. Lin, J. F. Lu, C. X. Xu, Y. Y. Wang, Z. L. Shi, J. Dai, *ACS Nano* **2015**, *9*, 6794.
[35] X. D. Wang, P. Wang, J. L. Wang, W. D. Hu, X. H. Zhou, N. Guo, H. Huang, S. Sun, H. Shen, T. Lin, M. H. Tang, L. Liao, A. Q. Jiang, J. L. Sun, X. J. Meng, X. S. Chen, W. Lu, J. H. Chu, *Adv. Mater.* **2015**, *27*, 6575.
[36] J. M. Lee, J. W. Choung, J. Yi, D. H. Lee, M. Samal, D. K. Yi, C. H. Lee, G. C. Yi, U. Paik, J. A. Rogers, W. I. Park, *Nano Lett.* **2010**, *10*, 2783.
[37] B. Nie, J. G. Hu, L. B. Luo, C. Xie, L. H. Zeng, P. Lv, F. Z. Li, J. S. Jie, M. Feng, C. Y. Wu, Y. Q. Yu, S. H. Yu, *Small* **2013**, *9*, 2872.
[38] J. H. Lee, E. K. Lee, W. J. Joo, Y. Jang, B. S. Kim, J. Y. Lim, S. H. Choi, S. J. Ahn, J. R. Ahn, M. H. Park, *Science* **2014**, *344*, 286.
[39] Y. K. Lin, H. W. Ting, C. Y. Wang, S. J. Gwo, L. J. Chou, C. J. Tsai, L. J. Chen, *Nano Lett.* **2013**, *13*, 2723.
[40] K. L. Kelly, E. Coronado, L. L. Zhao, G. C. Schatz, *J. Phys. Chem. B* **2003**, *107*, 668.
[41] X. Miao, S. Tongay, M. K. Petterson, K. Berke, A. G. Rinzler, B. R. Appleton, A. F. Hebard, *Nano Lett.* **2012**, *12*, 2745.
[42] L. B. Luo, W. J. Xie, Y. F. Zou, Y. Q. Yu, F. X. Liang, Z. J. Huang, K. Y. Zhou, *Opt. Express* **2015**, *23*, 12979.
[43] J. S. Jie, W. J. Zhang, Y. Jiang, X. M. Meng, Y. Q. Li, S. T. Lee, *Nano Lett.* **2006**, *6*, 1887.
[44] G. Konstantatos, M. Badioli, L. Gaudreau, J. Osmond, M. Bernechea, G. D. A. Fp, F. Gatti, F. H. Koppens, *Nat. Nanotechnol.* **2012**, *7*, 363.
[45] G. Konstantatos, J. Clifford, L. Levina, E. H. Sargent, *Nat. Photonics* **2007**, *1*, 531.
[46] S. Liu, Z. M. Wei, Y. Cao, Z. X. Wang, W. Xu, X. F. Guo, D. B. Zhu, *Chem. Sci.* **2011**, *2*, 796.
[47] Q. Q. Lin, A. Armin, D. M. Lyons, P. L. Burn, P. Meredith, *Adv. Mater.* **2015**, *27*, 2060.
[48] L. Dou, Y. Yang, J. You, Z. Hong, W.-H. Chang, G. Li, Y. Yang, *Nat Commun.* **2014**, *5*, 5404.
[49] N. Su, R. Rajavel, P. Deelman, J. N. Schulman, P. Fay, *IEEE Electron Device Lett.* **2008**, *29*, 536.
[50] G. Y. Xu, A. Salvador, W. Kim, Z. Fan, C. Lu, H. Tang, H. Morkoc, G. Smith, M. Estes, B. Goldenberg, W. Yang, S. Krishnankutty, *Appl. Phys. Lett.* **1997**, *71*, 2154.
[51] J. M. Liu, *Photonic Devices*, Cambridge University Press, Cambridge **2005**.
[52] J. S. Jie, W. J. Zhang, Y. Jiang, X. M. Meng, Y. Q. Li, S. T. Lee, *Nano Lett.* **2006**, *6*, 1887.
[53] D. D. Lin, H. Wu, W. Zhang, H. P. Li, W. Pan, *Appl. Phys. Lett.* **2009**, *94*, 172103.
[54] K. Liu, M. Sakurai, M. Liao, M. Aono, *J. Phys. Chem. C* **2010**, *114*, 19835.
[55] H. Lim, S. Tsao, W. Zhang, M. Razeghi, *Appl. Phys. Lett.* **2007**, *90*, 131112.
[56] T. Y. Duan, C. N. Liao, T. Chen, N. Yu, Y. Liu, H. Yin, Z. J. Xiong, M. Q. Zhu, *Nano Energy* **2015**, *15*, 293.
[57] Y. Arslan, T. Colakoglu, C. Besikci, *IEEE J. Quantum Electron.* **2013**, *49*, 186.
[58] A. V. Uskov, I. E. Protsenko, R. S. Ikhsanov, V. E. Babicheva, S. V. Zhukovsky, A. V. Lavrinenko, E. P. O'Reilly, H. X. Xu, *Nanoscale* **2014**, *6*, 4716.

© 2016 WILEY-VCH Verlag GmbH & Co. KGaA, Weinheim